# CARBON NANOSPHERE ELECTRODES FOR LITHIUM SULFUR BATTERIES

A Thesis

Presented to the Faculty of the Graduate School

of Cornell University

in Partial Fulfillment of the Requirements for the Degree of

M.S.

by

Steven D. Kiekel

August 2016

## ABSTRACT

A synthesis method for self-assembled hollow carbon spheres was developed for use as a sulfur support in lithium sulfur batteries, with the goal of reducing polysulfide dissolution during the charge/discharge cycle. The resulting carbon is approximately 8% graphitic with high surface area ($2000 m^2/g$) and 4nm diameter pores throughout the spheres. The diameter of the spheres is between 150 and 200nm, without any strong correlation to the synthesis parameters used. The spheres were imaged using electron microscopy techniques, and the elemental composition determined using Energy-Dispersive X-ray spectroscopy. Raman spectroscopy was employed to measure the carbon content, and the conductivity of the samples were measured. TEM analysis showed that the spheres were not hollow as intended, but porous throughout. The spheres were infused with sulfur and used as the cathode in lithium sulfur coin cell batteries, whose energy storage capacities were tested over 250 cycles.

## BIOGRAPHICAL SKETCH

Steven Kiekel received an AS in Engineering Science in 2009 and a BS in Physics from Ithaca College in 2012, where he received departmental honors for his academic and research endeavors. As an MS student in Applied Physics at Cornell, he served as Chief Engineer and team lead for Resistance Racing, a project team in the electrical engineering department building an electric motorcycle. It was the same passion for battery technology that led to this research topic. After receiving his MS from Cornell, he will be joining Z-Senz, a startup company founded by other Applied and Engineering Physics graduate students building LIDAR distance sensors.

## ACKNOWLEDGEMENTS

This work was completed with the help of many people from across the Cornell campus. Led by Prof. Giannelis, our group has been invaluably helpful in this endeavor. Baoquan Xie developed the initial synthesis method and Ritu Sahore developed the lithium sulfur battery technique. Turki Baroud contributed invaluable assistance with labwork and analysis. Mian Pan assisted in measuring the conductivity of the carbon, and Zhengyuan Tu aided with the battery capacity measurement. Prof. Muller served as a committee member and academic advisor, Kit Umbach assisted with the Raman spectroscopy, and Barnaby Levin performed the TEM imaging. This work made use of the Cornell Center for Materials Research Shared Facilities which are supported through the NSF MRSEC program (DMR-1120296). The author would also like to thank his family for their support, which made this time at Cornell possible. Special thanks to Emily, Alex, Reet, Max, Mingtong, and Albert for providing some sanity when it was in short supply.

## TABLE OF CONTENTS

## LIST OF TABLES

## LIST OF FIGURES

CHAPTER 1

# INTRODUCTION

Lithium Sulfur batteries were proposed and developed as early as 1968 and have long been considered as an option for widespread commercial use [25]. Several factors have contributed to the prevention of their use however, notably safety concerns, and loss of capacity due to polysulphide formation[1]. The current industry standard for electrical energy storage utilizes lithium ion technology, and can be found everywhere from smartphones to electric vehicles.

## 1.1 Lithium Ion Batteries

Lithium ion technology is currently the primary choice in industry for energy storage in a wide variety of applications, from cell phones and laptops to electric vehicles. Advancement in the technology has progressed rapidly in the last decade, spurred on by the need for ever higher energy storage in ever smaller and lighter packaging. As a result, entirely new technologies and industries have developed that were not previously possible.

Lithium ion energy storage is accomplished through a process known as topotactic intercalation, in which lithium ions are transported through an electrolyte into a solid electrode without causing significant change to the electrodes physical structure, as illustrated in Fig. 1.1. The positive electrode (cathode) typically consists of a lithium transition metal oxide, while the negative electrode (anode) is generally carbon, with a potential of around 3.3V between the two, depending on the materials. At its most basic, the anode is a solid block of graphite, which recent advancements have improved by using nanostruc-

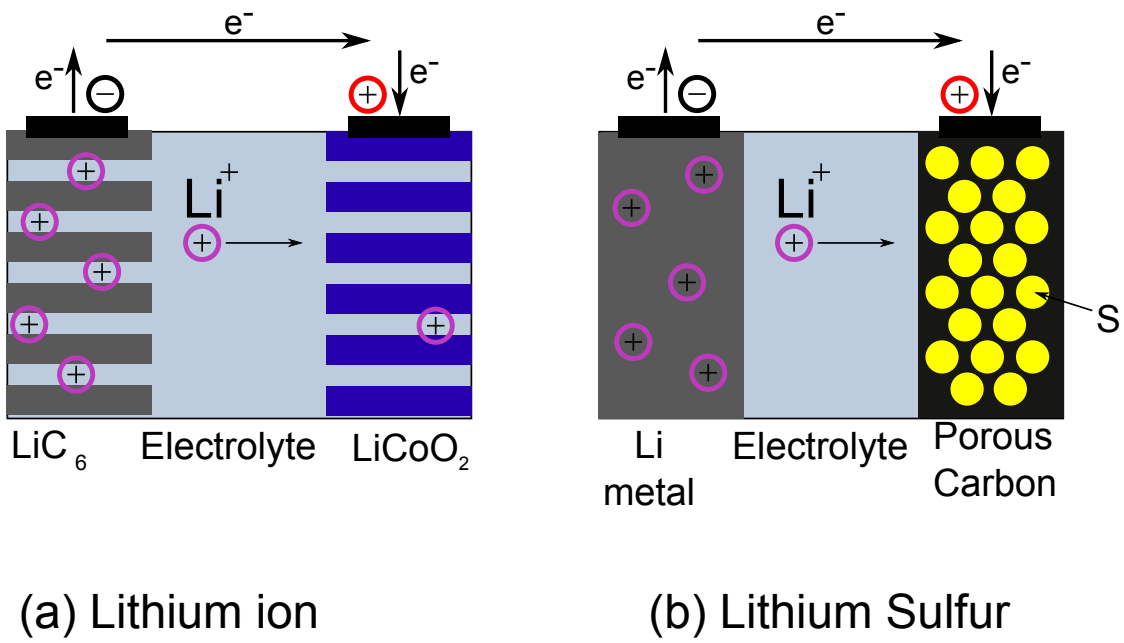


Figure 1.1: Illustration of energy storage technologies. (a)Lithium ion batteries store charge through the intercalation of lithium atoms in and out of the electrodes. (b)Lithium sulfur batteries store charge through the reversible chemical combination of lithium and sulfur.

tured carbon architectures. The theoretical maximum charge storage capacity for lithium ion technology is 300 mAh/g, while actual devices have been built with capacities as high as 200 mAh/g [12]. For comparison, the Panasonic NCR18650 cell is used heavily in many applications, and has a capacity of 58 mAh/g or 211 Wh/kg, roughly 20% of the theoretical maximum [23].

## 1.2 Lithium Sulfur Batteries

Lithium sulfur batteries rely on a completely different chemical process to store and deliver charge. Lithium atoms are dissolved from the anode, which is solid lithium metal, and carried across the electrolyte to cathode. The cathode is a

porous carbon which is loaded with sulfur that is reduced during discharge, forming polysulphide chains. The idea of loading the sulphur into porous carbon originated in the 1980's, with Peled et al. using carbon to increase electrical conductivity and improve energy density[35]. The polysulphides react with the lithium in a 2:1 ratio to form $Li_2S$. This reaction occurs across a potential of around 2.2V. The theoretical charge storage limit to this reaction is 1166mAh/g, roughly four times that of lithium ion devices. One large reason for this difference is the difference in materials. Lithium, as the lightest metal, makes an ideal cathode material in this respect, as lithium ion batteries often use oxides based on dense metals such as iron and cobalt.

In practice, devices have been built with capacities as high as 160mAh/g, with values as high as 272mAh/g expected in the near future [22]. The significant difference between the theoretical and practical energy density is a result of several factors. First, the carbon structure which contains the sulfur and acts as an electrical conductor is not accounted for in the calculation, as it does not directly contribute to the Li-S reaction. The lithium anode also must contain significantly more material than in the ideal case due to the inefficiency of the reaction. This extra mass, plus the mass of the packaging results in a reduced energy storage density[1].

One major problem that has plagued lithium sulfur battery technology from its inception has been the dissolution of the polysulphides into the electrolyte[4]. This problem can be exacerbated by the physical damage to the cathode caused by mechanical stress from the expansion and contraction of the sulfur as it reacts with the lithium ions. This can lead to a variety of issues, including low efficiency when charging, high self-discharge rate, and safety concerns. The is-

sue that this work aims to address is the tendency for capacity to fade as the cell is charged and discharged repeatedly. Dissolved sulfur can drift across the electrolyte and react with the lithium anode irreversibly, reducing the available reaction constituents and charge storage capacity.

A variety of attempts have been made to trap the sulfur in the cathode, notably the use metal oxides[10][6] or conducting polymer[34] [38] additives and the use of porous carbon cathodes. The use of porous carbon allows the sulfur to be contained and protected from dissolution within a highly conductive structure. The carbon can take many forms, including amorphous carbon black[37], graphene and graphene oxides[2][3], carbon nanotubes[40], and macro-, meso-, and micro-porous carbon[16][18]. In this work, sulfur is encapsulated within the pores of hollow carbon spheres, as illustrated in Fig. 1.2.

The performance of the cells can be optimized by finding the ideal balance between four main factors: sulfur content, penetration of electrolyte and lithium into the sulfur, electron conduction out of the sulfur, and sulfur dissolution out of the cathode. Performance in a cell is increased by maximizing these factors, with the exception of the last, sulfur dissolution, as mentioned above. Sulfur content leads directly to energy storage capacity, as it provides more reactants for the LiS reaction, which requires that the lithium have access to the sulfur through the electrolyte. The sulfur itself is electrically insulating, so it is vital that contact between the sulfur reactant and the conducting carbon is maximized. By varying the inner diameter and shell thickness of the spheres, these performance factors can be maximized[9].

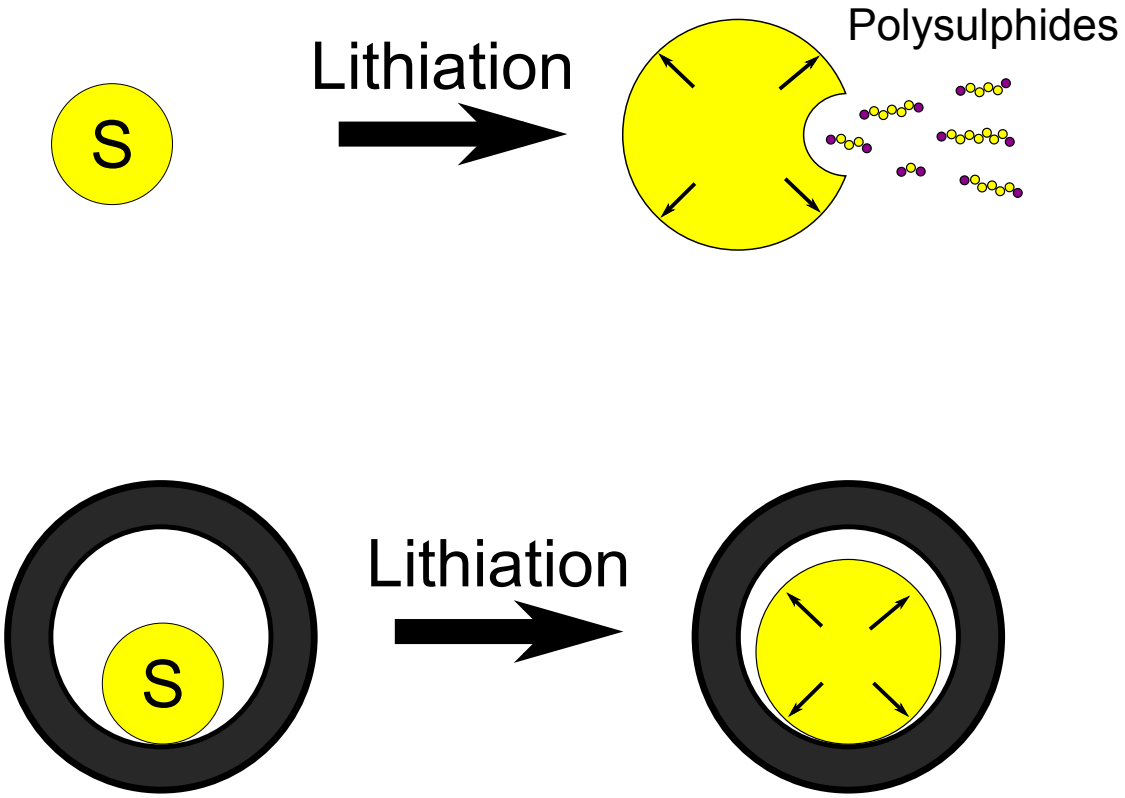


Figure 1.2: Upon reacting with lithium ions, sulfur breaks into polysulphide chains which can dissolve into the electrolyte, reducing energy storage capacity. By encapsulating the sulfur in carbon spheres, the sulfur can react while minimizing capacity loss.

CHAPTER 2

# METHODS

A synthesis method was developed for producing carbon spheres varying in diameter from 100nm to 500nm. Originally, the method was intended to produce hollow spheres with varying inner and outer diameter, but after characterization it became clear that the resulting product was not hollow, but porous.

## 2.1 Synthesis

In a 500mL Erlenmeyer flask, a solution of Triton X-100 (or NP-10), Pluronic F-127, and NaCl was dissolved in 150mL of deionized (DI) water in a 1.5:0.75:1.0 respective ratio by mass. Simultaneously, 4.0g of Melamine is dissolved in a 100mL round bottom flask with 6.35mL formaldehyde, 20mL DI water, and 5 drops of 1M $Na_2CO_3$. The solution is stirred in an oil bath at 70°C until all solids are dissolved and liquid is clear, usually 30-45 minutes.

Melamine/Formaldehyde (MF) solution is poured into the 500mL Erlenmeyer flask containing the F-127 and NP-10 solution, pouring slowly to avoid creating bubbles. Five drops of 1M citric acid is added to balance the pH and the solution is stirred in a 70°C oil bath until the solution becomes visually cloudy. It is at this point that the inner MF prepolymer is forming which will form the inner core of the hollow sphere upon carbonization in the furnace[8][26]. The opacity of the solution is indicative of the size of the prepolymer spheres, which grow larger the longer the reaction is allowed to continue. The rate at which this self-assembly occurs is inversely related to the pH of the solution; two or three additional drops of citric acid can be added to accelerate the process if no

opacity change is visible after two hours.

Once the desired opacity is reached, Resorcinol is added to the desired ratio. For this experiment, 0.7g, 1.0g, or 1.3g was used. 75mL of ethanol is then added, along with 1mL of formaldehyde and 1mL of ammonia hydroxide. The solution is then left stirring in a 70°C oil bath for 12-18 hours. Typically the solution becomes slightly less cloudy as the ethanol is added, as the MF spheres become more dispersed in the solution. The color of the solution is initially clear to white, depending on the reaction time. As the ammonia hydroxide is added, the solution takes on a yellow tint which darkens to a light red/tan color over the course of the reaction[21].

The desired result is a suspension of slightly reddish, light tan solid in clear liquid. The solids are filtered using a Buchner funnel with 50$\mu$m filter paper, then rinsed and re-filtered twice using 1 litre of DI water. In early experiments, the solid was then placed on aluminum foil and dried in a 60°C drying oven, but later experiments utilized a low pressure freeze dryer. Freeze drying the solid was found to produce a more consistent, powdery material in contrast to the hard flakes produced from the drying oven.

The first round of experiments sought to vary the size of the inner compartment by varying the reaction and formation time of the RF inner core[20][19]. In addition, the ratio of RF/MF was varied to adjust the thickness of the MF outer shell.In the second round, the RF formation was allowed to continue until the opacity of the solution changed from clear to opaque. This should indicate the size of the spheres, which scatter progressively more light as they increase in size. The expected result for both experiments is therefore a variety of spheres with varying inner and outer diameters[32].

## 2.2 Carbonization/Activation

After synthesis, the sample is transferred to a crucible boat for carbonization. The crucible is placed in a Marshall tube furnace with a nitrogen gas atmosphere, and the temperature is increased at a rate of 5°C/min until 900°C is reached. This temperature is held for two hours, then the furnace is shut off and the sample is allowed to cool. Once the sample has cooled enough to handle (below 200°C), it is transferred to a Lindberg tube furnace with a $CO_2$ atmosphere and run through an identical heating profile. The result should be a fine, black powder with very low mass density[7][30].

It is possible to use the Lindberg furnace to complete both carbonization in nitrogen atmosphere and activation in $CO_2$, and it was initially thought that the two steps could be combined by ramping up to 900°C in nitrogen atmosphere, holding for two hours, then switching to $CO_2$ for two hours. This protocol was attempted, but the resulting solid was consistently hard and silver-grey. It was found that separating the two processes and providing a high nitrogen and $CO_2$ flow ensured the most consistent results.

## 2.3 Sulfurization

Sulfur must now be added to the carbon spheres. For this experiment, sulfur was added in a 1:1 ratio to the carbon by mass. It was found that using 50mg of each produced a convenient amount of carbon/sulfur (CS) for electrode assembly, with aluminum foil used in place of weigh paper to prevent static buildup and sticking. The CS mixture is then mixed in a mortar and pestle until uniform,

at which point it forms “sheets”.

The CS mixture is then put into a sealed crucible to prevent the sulfur from sublimating out and placed in an oven at 160°C for 18 hours. The viscosity of sulfur has been shown to be miniimized at this temperature, allowing it to ideally penetrate into the pores of the carbon spheres[18]. Sulfur absorption and penetration was confirmed using TEM x-ray analysis.

## 2.4 Electrode Assembly

The CS composite is next suspended in a slurry consisting of 80% CS, 12% carbon black, and 8% binder by weight. The CS and carbon black (Super P) are both weighed on aluminum foil as before and combined in a mortar and pestle. The binder used is polyvinyledene fluoride (PVDF), and is dissolved to 2% by weight in N-Methyl-2-pyrrolidone (NMP) solvent solution. The PVDF/NMP solution is weighed into the crucible by placing the solution’s bottle and a transfer pipette on a scale and taring it. Drops are then added to the mortar via the pipette, and the weight read as the negative value on the scale when the pipette is replaced.

After mixing the CS, carbon black, and binder, more NMP solvent is added and mixed into the mortar until the slurry reaches a viscosity roughly that of honey. A thin piece of aluminum foil roughly 10cm wide and 15cm long is then placed on a glass sheet and smoothed using a Kim Wipe and ethanol. The slurry is placed on the aluminum and spread using a doctor blade. The doctor blade is pulled across the aluminum, evenly spreading the slurry at a thickness of 20$\mu$m. Once an even layer of the slurry has been spread, the glass sheet and aluminum

foil are placed in an oven at 60°C for 15-20h to evaporate the NMP and any moisture. This process, including the drying oven, is performed under a fume hood due to NMP's volatility and toxicity.

## 2.5 Coin Cell Assembly

To test the performance of the CS compound in a lithium sulfur battery, the slurry is used as the cathode in a CR2032 coin cell battery. First the aluminum foil is placed on a large weigh paper with the CS material down. A 5/8" punch and a hammer are used to make the electrode discs for the battery. Each electrode is weighed, subtracting the weight of the aluminum to find the mass of the sulfur. The electrodes are then placed back in a 70°C oven to drive off any remaining solvent or moisture, which could react with the lithium during assembly.

Because the anode in a lithium sulfur battery is solid lithium metal, the assembly of the coin cell must take place inside an argon atmosphere glove box. The electrodes and other components are placed in the airlock and evacuated three times to replace the air with argon. The coin cell consists of eight components which must be assembled in order. The bottom cap of the CR2032 cell holds the cathode in place, providing an electrical connection between the battery terminal and the aluminum electrode backing. The CS electrode disc is placed in the bottom cap with the carbon and sulfur composite facing up. A 3/4" diameter disc of 25$\mu$m Trilayer polypropylene-polyethylene-polypropylene membrane is used as the separator, placed over the cathode. 1 M Lithium Bis (Trifluoromethanesulfonyl) Imide (LiTFSi) (Sigma Aldrich) and

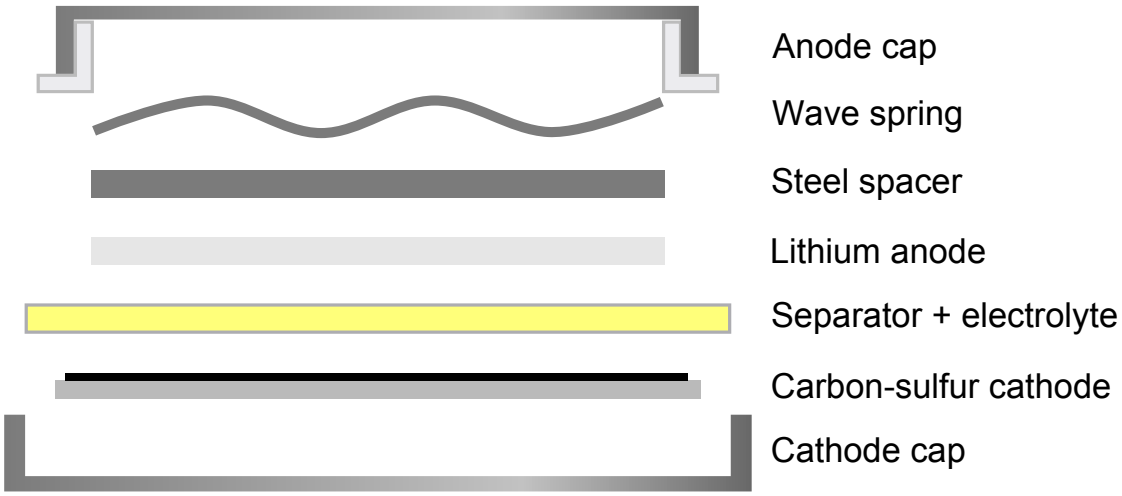


Figure 2.1: Illustration of battery cell components for CR2032 coin cell. The battery must be assembled in an argon atmosphere glove-box due to the reactivity of the lithium anode.

1wt% lithium nitrate (LiNO3) dissolved in a mixture of 1, 3-Dioxolane (DOL) and Dimethoxyethane (DME) (1:1 by volume) was used as the electrolyte, which is added to the separator[29]. Solid Lithium metal is cut from a strip using a 1/2" punch to form the anode. A stainless steel spacer and wave spring are placed above the lithium anode to ensure good electrical and mechanical contact with the anode and the top cap of the coin cell casing, which seals the battery. The components are assembled in the order presented, as illustrated in Fig.2.1. An electric crimping machine presses the two caps together, sealing the cell.

## 2.6 Characterization

### 2.6.1 Imaging

Imaging of the spheres was accomplished using both a Scanning Electron Microscope (SEM), and a Transmission Electron Microscope (TEM). Both methods utilize focused beams of electrons to produce high magnification images. SEM imaging is considerably simpler to carry out, but lacks the resolution of TEM. It was therefore used as a preliminary method of measuring the size of the spheres. TEM analysis allows for higher resolution, with the added benefit of imaging the internal structure of the spheres.

The TEM can also employ Energy-Dispersive X-ray (EDX) spectroscopy, providing a spectral analysis of scattered x-rays which can be used to determine the elemental composition of a sample. EDX was used to analyze the efficacy of the sulfur melt-infusion into the carbon spheres. To estimate how far the sulfur has penetrated, a linescan was performed across one of the spheres, analyzing the intensity of x-rays in the carbon and sulfur regimes. Using this data, the ratio of sulfur to carbon content can be found through the sphere, indicating the depth of sulfur penetration[28].

To measure the carbon and suflur composition analytically, we must relate the intensity of x-rays emitted at the characteristic frequencies of carbon and sulfur, $I_C$ and $I_S$, to the concentration of each element, $C_C$ and $C_S$. This is accomplished by the Cliff-Lorimer factor $k_{CS}$ in the equation

$$\frac{C_C}{C_S} = k_{CS}\frac{I_C}{I_S} \tag{2.1}$$

or

$$k_{CS} = \frac{C_C}{C_S}\frac{I_S}{I_C}. \tag{2.2}$$

$k_{CS}$ is particular to the particular TEM device used, and can be determined from previous measurements.

### 2.6.2 BET

The surface area and pore volume of the samples was measured using a Micromeritics ASAP2020, which utilizes Brunauer Emmett Teller (BET) and Barrett Joyner Halenda (BJH) models. Nitrogen adsorption and desorption isotherms and pore size distributions were obtained at 77K using liquid nitrogen.From these measurements, the surface features of the carbon sample can be determined, including the average surface area per gram of material and the distribution of pore sizes throughout[5][36].

### 2.6.3 RAMAN

Raman spectra was obtained using a Renishaw InVia Confocal Microscope with a 488nm laser at 10% power. Data was collected using exposure times of 10 and 40 seconds. For carbon, the G- and D-Raman peaks can be observed at 1580 and 1350cm$^{-1}$ respectively. By comparing the intensity and area under each peak, the graphitic content of the carbon can be determined. The high electrical

conductivity of graphite compared to amorphous carbon makes it desirable to have high graphite content[9][14].

### 2.6.4 Conductivity

The conductivity of the carbon spheres was measured by compressing the sample between brass electrodes with leads running from the ends of the sample. By connecting this in series with a known resistance $R$ and a voltage supply $V_{source}$ , a voltage divider is formed. The voltage across the sample $V_{sample}$ is given by

$$V_{sample} = V_{source}\frac{R}{R + R_{carbon}} \tag{2.3}$$

where $R_{carbon}$ is the resistance of the carbon sample. Observing that the sum of the voltages across the sample and the resistor must equal the source voltage and rearranging gives

$$R_{carbon} = R\frac{V_R}{V_{sample}}. \tag{2.4}$$

The above equation allows the resistance of the sample to be calculated by measuring $V_R$, $V_{sample}$, and $R$. The conductance $\sigma_{carbon}$ is given by the equation

$$\sigma_{carbon} = \frac{l}{R_{carbon}A} \tag{2.5}$$

where $l$ and $A$ are the length and area respectively of the particular sample.

The sample carbon is packed into a 1.98mm diameter hole in a nylon block. Brass plugs are then placed on either end, compressing the carbon. Electrodes inside the hole are placed such that they make contact with the sample material and are separated by 1.5mm. By connecting leads to the brass plugs, a current can be passed through the sample, while the voltage across the sample can be measured. By placing this assembly in series with a voltage source and resistor, the resistance and thus conductance of the sample can be measured. Fig. 2.2 illustrates the apparatus.

### 2.6.5 Battery Capacity

The capacity of the coin cell batteries was measured over 250 galvinostatic charge/discharge cycles with a voltage range of 1.7-2.8V. One of the samples continued testing through 1000 cycles. All experiments were carried out at 1C, meaning that each charge/discharge cycle took one hour to complete. The measured capacity of the battery is divided by the mass of the sulfur present to produce the specific capacity of the electrode in units of $mAh/g$.

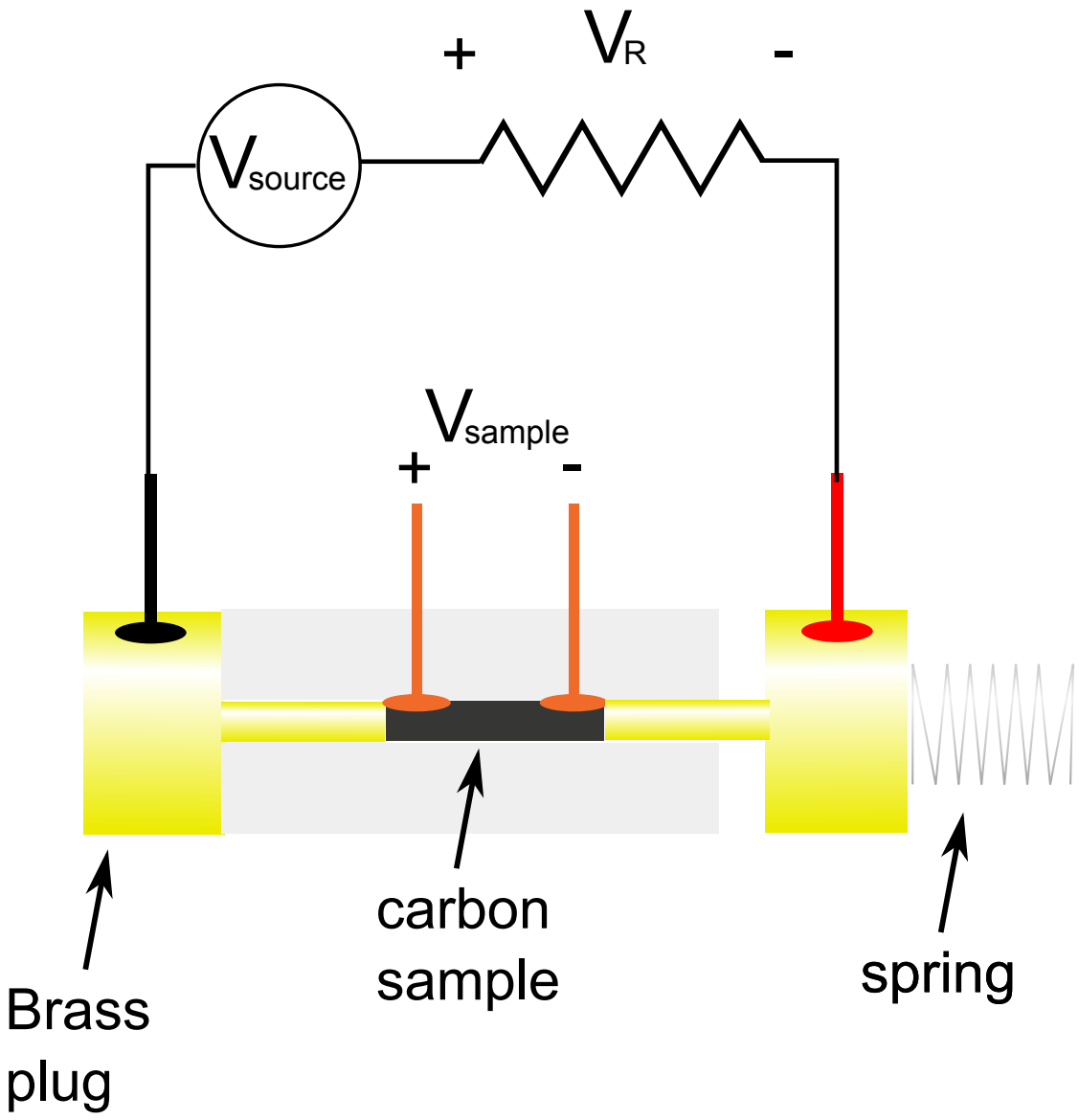


Figure 2.2: The conductivity of the carbon sample is measured by connecting it in series with a known resistance and applying a voltage. The circuit acts a voltage divider, allowing the resistance of the carbon sample to be determined by comparing the voltage across the resistor ($V_R$) and across the sample ($V_{sample}$).

CHAPTER 3

# RESULTS

## 3.1 Imaging

Initial experiments sought to tune the sphere size by varying the length of time the reaction is carried out while maintaining the pH of the reaction. Tests were carried out with three different MF/RF ratios: 4.0:0.7, 4.0:1.0, and 4.0:1.5. For each MF/RF ratio, the time of the MF prepolymer reaction was varied from one to two hours in 15 minute increments. The expected result was a series of hollow spheres with varying inner diameter (due to the MF reaction time) and varying shell thickness (due to the MF/RF ratios). Initial analysis was carried out using a TESCAN MIRA3 Scanning Electron Microscope (SEM), and showed that not only were the sphere sizes relatively invariant, but many of the samples had formed aggregate materials from the spheres, resulting in large, amorphous masses in place of individual spheres. Examples of these images can be seen in Fig. 3.1.

The experimental procedure was changed to address both of these issues. In order to achieve more variety in the sphere size, the MF reaction was allowed to continue until the solution became visibly cloudy, indicating the formation of the prepolymer spheres. The opacity of the solution was thus used as a measure of the size of spheres, which scatter more light as they grow until the solution becomes fully opaque. The experiment was repeated as before, using identical MF/RF ratios. The pre-polymer solution was monitored during the reaction until it had reached the desired opacity, ranging from barely visibly cloudy to completely opaque. In the event that the solution had not become cloudy after 2

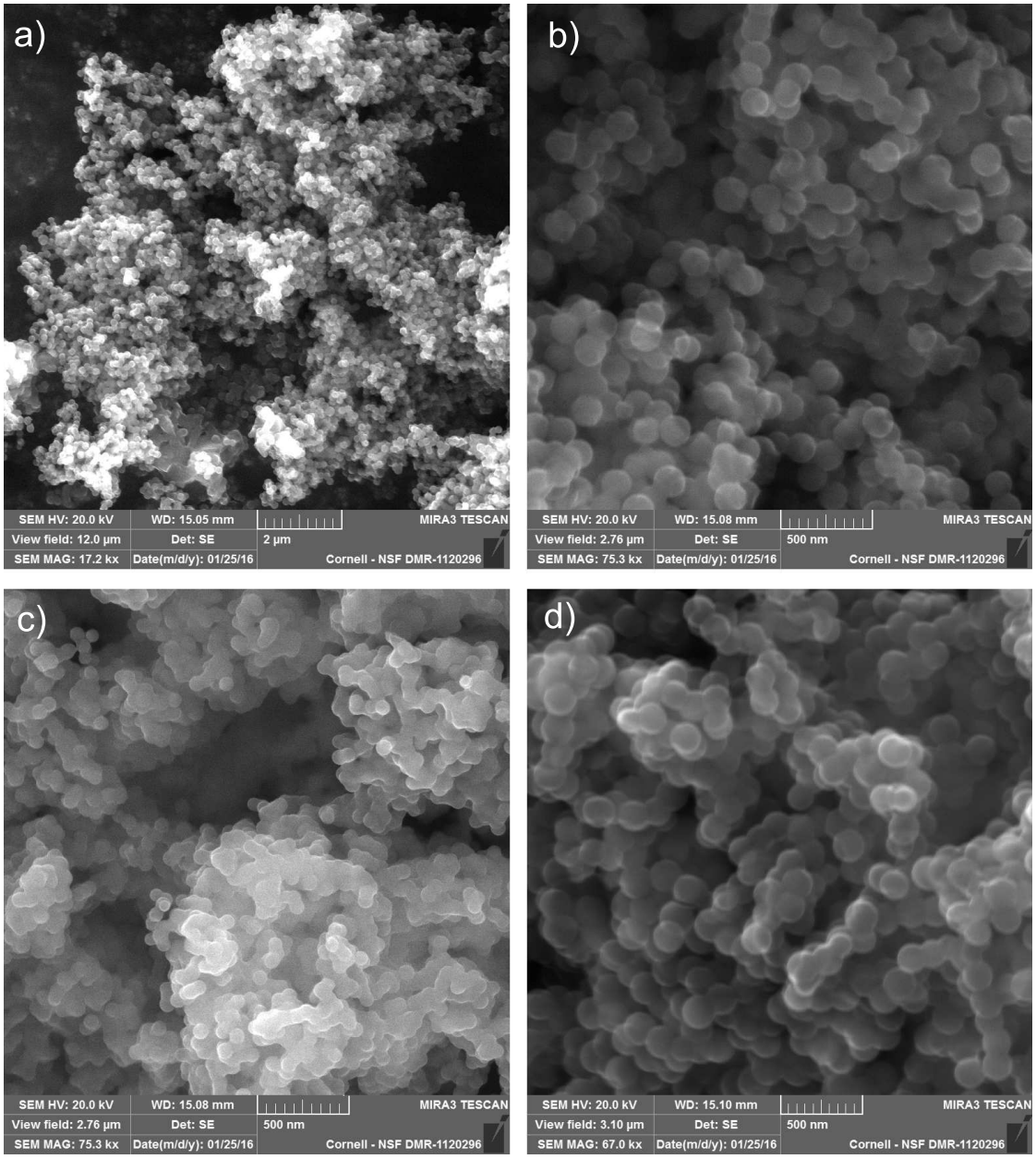


Figure 3.1: SEM images show that initial experiments produced aggregate material after carbonization and activation of the RF/MF polymer. Individual spheres range in diameter from 150-200nm, and can be seen to have fused together into a conglomerate. This is thought to be due to the drying process used after synthesis. *SEM imaging by Baoquan Xie.*

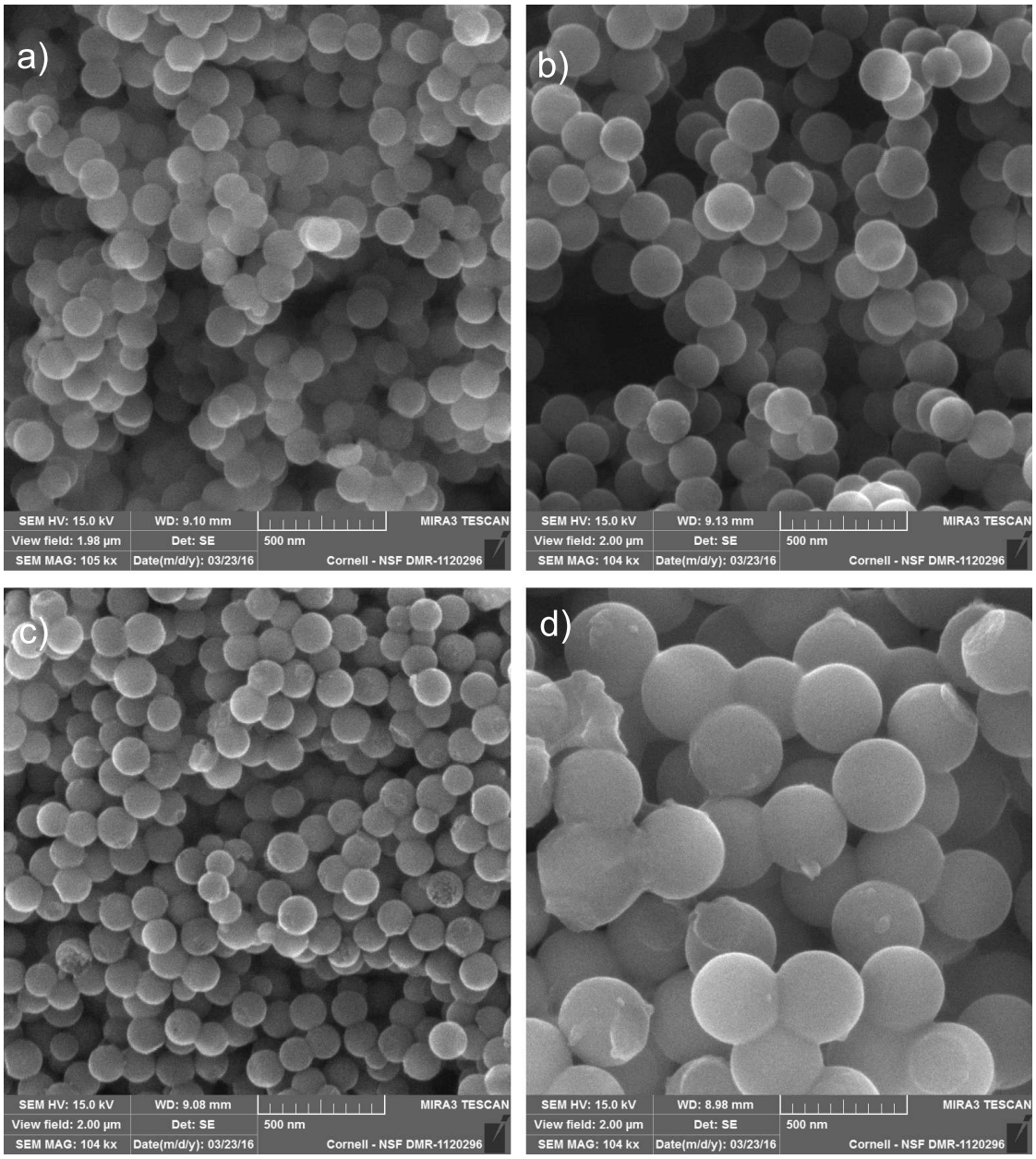


Figure 3.2: SEM images show individual spheres formed after carbonization and activation of the RF/MF samples. By using a freeze drying method under low vacuum, the spheres are kept from congealing into an aggregate. *SEM imaging by Baoquan Xie.*

hours, a few drops of citric acid were added to accelerate the reaction. The reaction time varied from two to five hours. To prevent the spheres from forming an aggregate, drying was moved from a 60°C oven to a vacuum freeze dryer. This step took substantially longer than oven drying, but resulted in better sphere formation. These samples are referred to using the convention x-y-z, where x and y represent the MF:RF ratio as x:y, and z represents the expected size due to the opacity, S, M, L, or XL. Additional SEM imaging was performed on the new samples to analyze the results, which can be seen in Fig. 3.2. There is some slight correlation between the observed opacity of the MF solution and the resultant sphere size, but all spheres produced using this method were between 140nm and 200nm in diameter with the exception of one outlier. Sample 04-10-S, which is expected to be on the small end of the spectrum, instead appears to have a diameter twice that of most of the other samples (Fig. 3.3). Other samples which were expected to be larger than most were found to be in the same 150-175nm range as the majority of the samples, sometimes on the small end of the spectrum.

Further analysis of the spheres was conducted using an FEI F20 Transmission Electron Microscope (TEM). TEM allows for better resolution than the SEM, as well as providing a view of the interior of the spheres and elemental spectrum analysis. Three samples and their respective carbon-sulfur compounds were imaged and studied, which can be seen in Figs. 3.4 and 3.5. The most striking finding from these images is that the spheres are not in fact hollow, but rather porous throughout. This morphology could explain the lack of variation in the size of the spheres found by SEM. Varying the size of the inner core obviously has no effect if the inner core is not present in the end result.

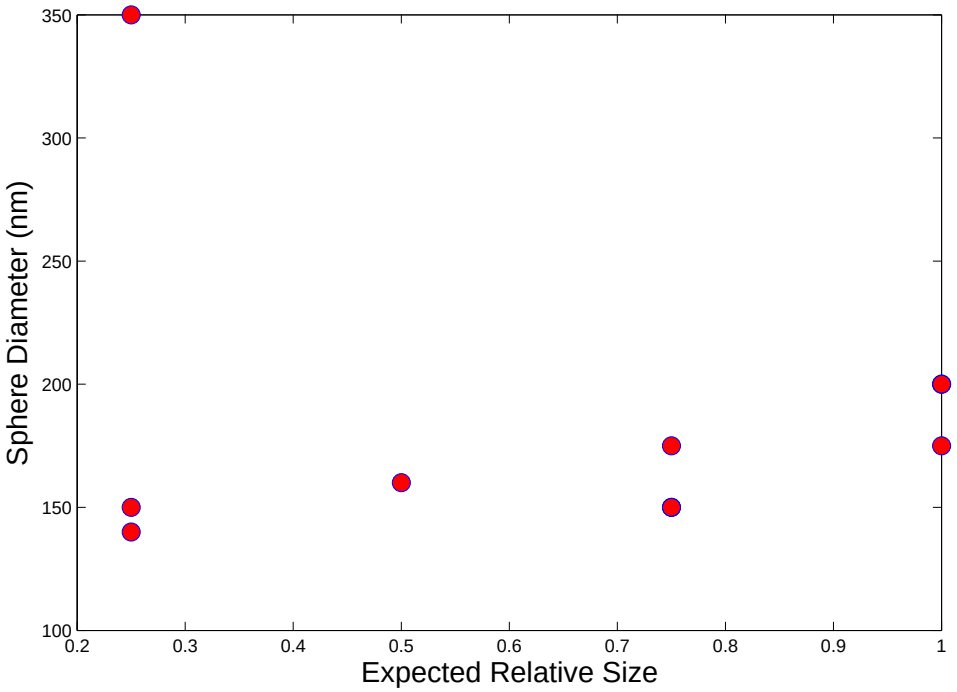


Figure 3.3: The diameter of the spheres was measured using SEM imaging and compared to the expected relative size due to the opacity of the MF pre-polymer solution. Most of the spheres were found to be in the 150-200nm range, with some small correlation to the expected size. One notable outlier was expected to be relatively small, but was instead found to be the largest diameter at 350nm.

### 3.1.1 Energy Dispersive X-Ray Spectroscopy

Fig. 3.5 shows the x-ray spectrum generated by the sample along with the spectral maps showing the location of carbon and sulfur in the sample. It can be seen that the sulfur has infused into the spheres. To estimate how far the sulfur has penetrated, a linescan was performed across one of the spheres, analyzing the intensity of x-rays in the carbon and sulfur regimes (Fig. 3.6). Using this data, the ratio of sulfur to carbon content can be found through the sphere, indicating

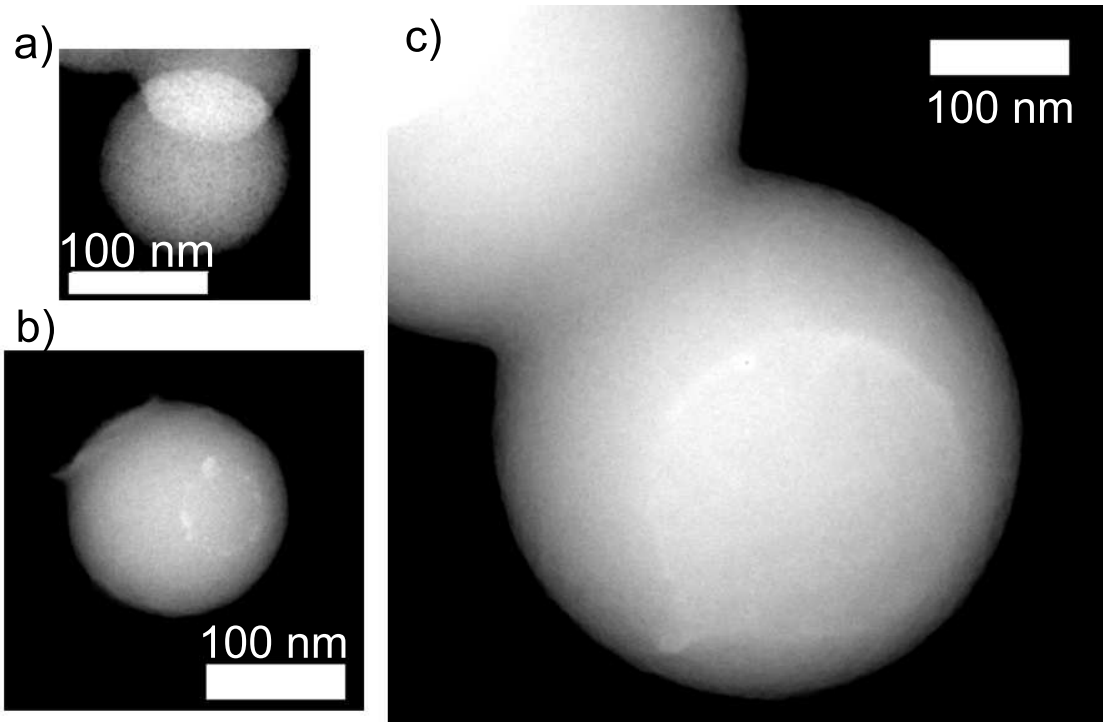


Figure 3.4: TEM imaging shows that the size of the spheres can be increased by varying the reaction time from a)4 hours to b)5.5 hours, or by changing the RF:MF reaction stoichiometry from a,b)4.0:0.7 to c)4.0:1.0. *TEM imaging by Barnaby Levin*

the depth of sulfur penetration.

Finding the intensity ratio $I_S / I_C$ can be accomplished by summing over the intensity profile for each elemental spectrum and dividing, which gives a value of 0.862[15]. The concentration ratio was found to be 2.55 from previous data obtained using the TEM. Multiplying the two as in eqn. 2.2 gives a value for $k_{CS}$ of 2.18.

After subtracting the background carbon signal, measuring the x-ray intensities as the beam is drawn across the diameter of the sphere produces Fig. 3.7. From this, the ratio of the intensities is taken and weighted by the Cliff-Lorimer constant.The result indicates that the sphere is roughly 55wt% carbon

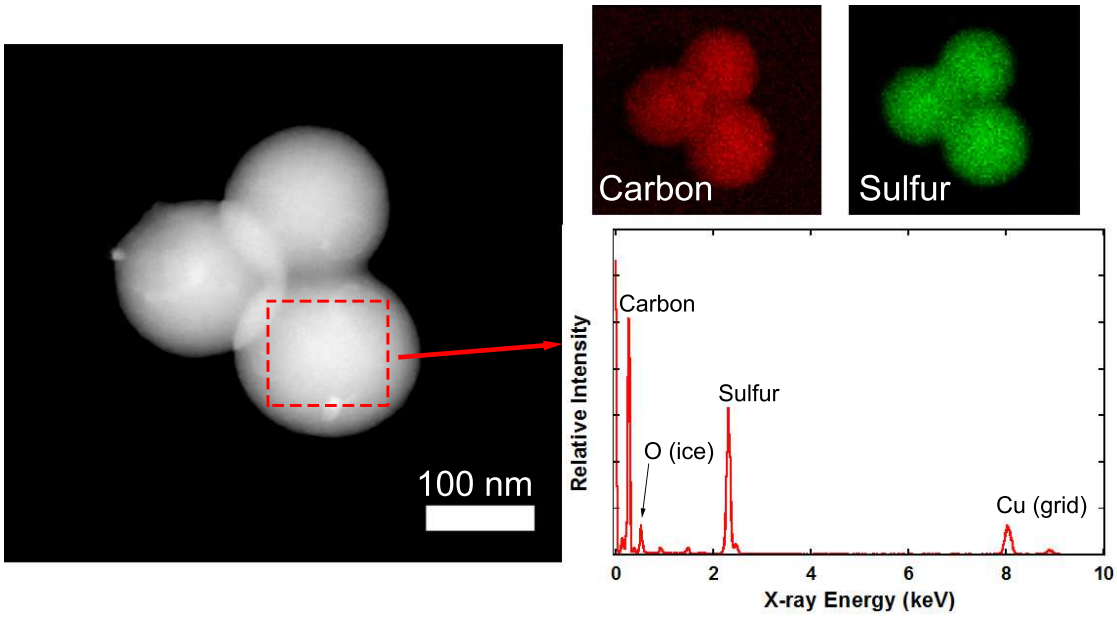


Figure 3.5: TEM x-ray analysis shows good, consistent sulfur (green) loading in the carbon (red) spheres. The intensity peaks show a roughly 50% loading by mass, as desired. *TEM imaging by Barnaby Levin*

and 45wt% sulfur. This result is consistent with the synthesis method, which used 1:1 C/S loading. Some sulfur loss is to be expected in the infusion process and from sublimation, which would account for the 5% difference.

## 3.2 Surface Area and Pore Size

The surface area and pore volume of the samples are measured using nitrogen adsorption and desorption isotherms obtained at 77K using liquid nitrogen, and are shown in Fig. 3.8. The isotherm plots show that there is little correlation between the opacity of the MF solution and the surface area of the resulting carbon. It is also worth noting the lack of space between the adsorption

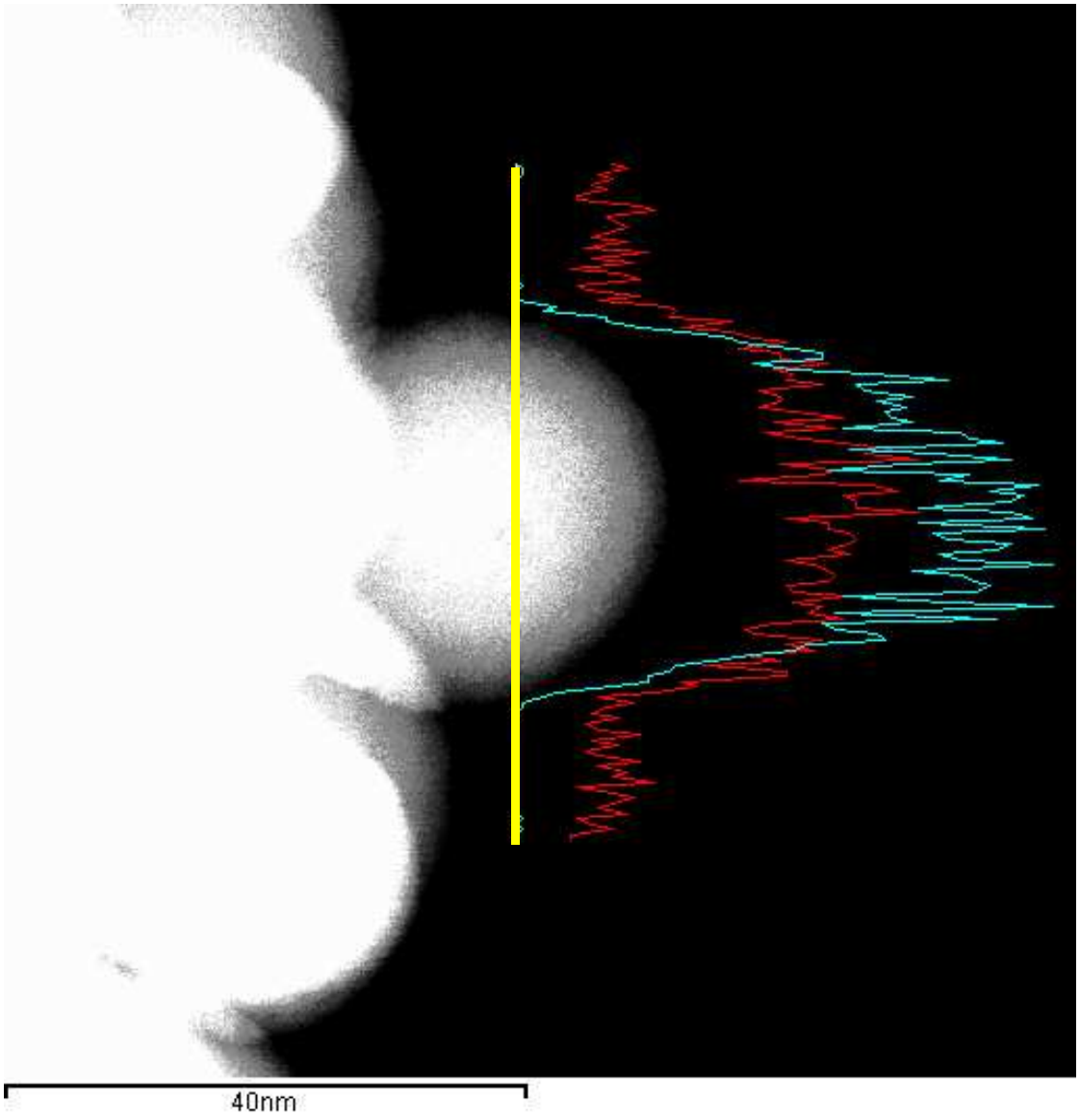


Figure 3.6: By drawing a TEM beam (yellow) across the diameter of a sphere and measuring the intensity of the x-ray radiation emitted in the carbon (red) and sulfur (blue) regime, the ratio of the two elements can be determined throughout the sphere.This indicates the efficacy of the sulfur melt-infusion process.

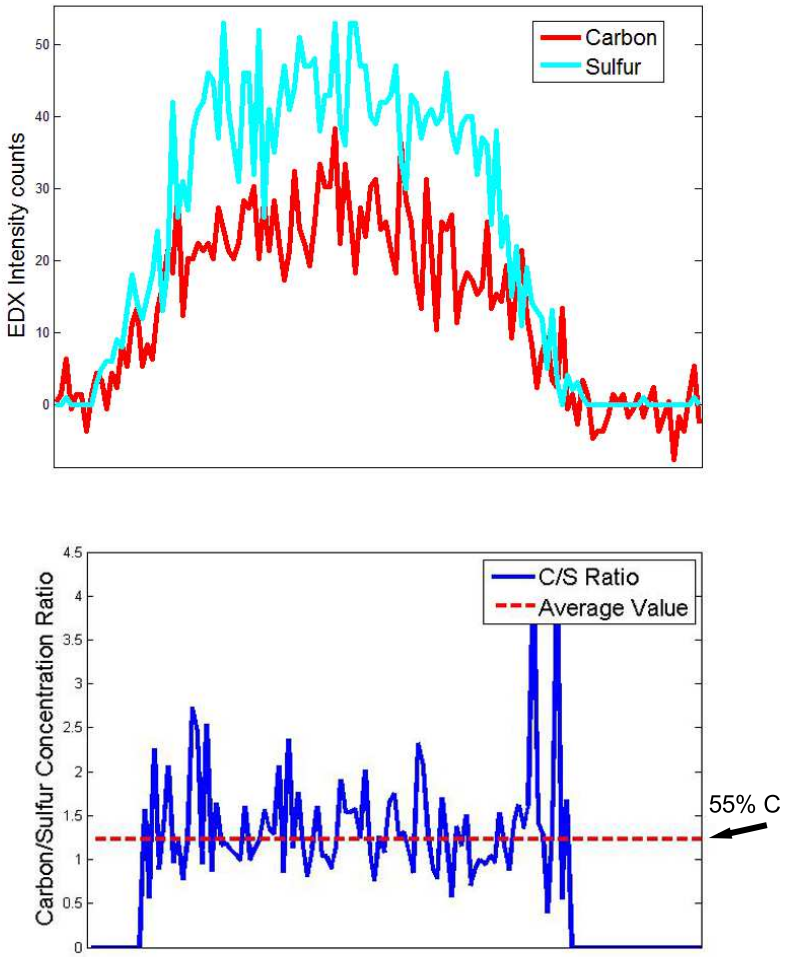


Figure 3.7: Analyzing the x-rays scattered by the sample in the TEM reveals the penetration of sulfur into the carbon spheres. Comparing the height of the intensity for the two elements (top), and weighting by the Cliff-Lorimer constant produces a ratio of the elemental concentration. The ratio of the carbon and sulfur intensity peaks shows that the average content of the spheres is 55% carbon and 45% sulfur, in agreement with the 50% mass ratio of the sulfur infusion process. The 5% difference can be attributed to the sublimation of the sulfur.

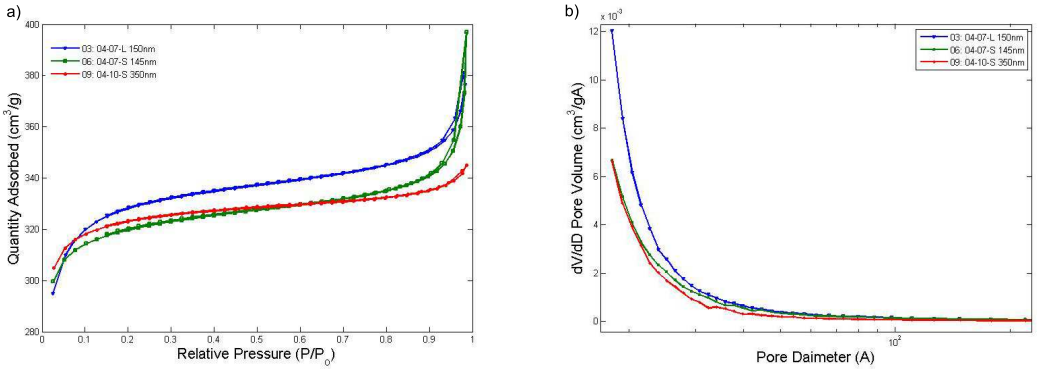


Figure 3.8: a)The adsorption-desorption isotherms and b)BJH pore size distributions were obtained at 77K using nitrogen sorption.

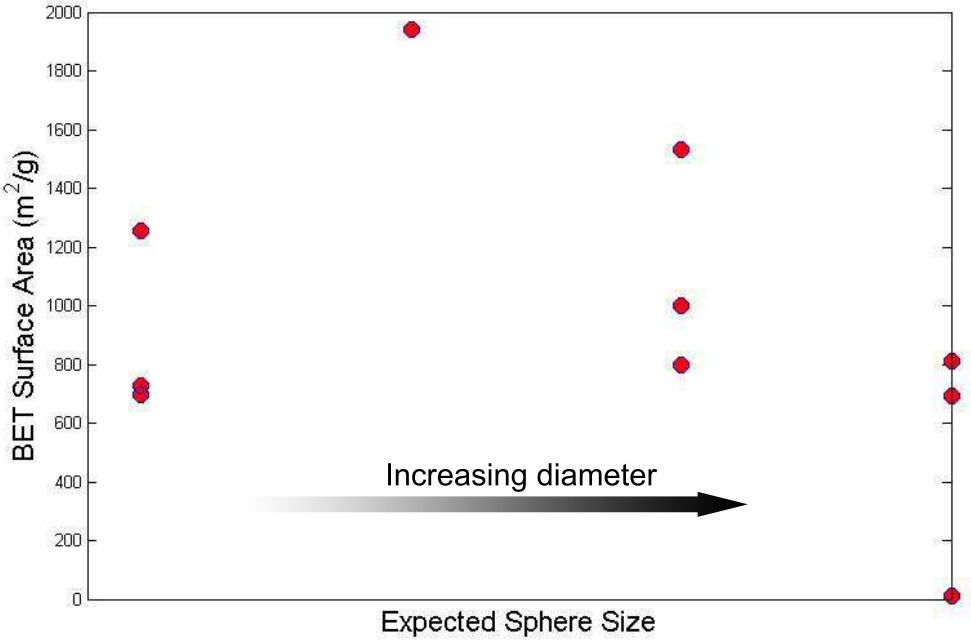


Figure 3.9: The BET surface area was compared to the predicted sphere size due to changes in the synthesis method, and no correlation was found. This is due in part to the lack of variety in the final sphere diameter across samples.

and desorption sections of the isotherm. This is another sign that there are no mesopores in the carbon, indicating that they are not hollow[11][39]. The pore size distribution reinforces this hypothesis, as it shows that very few pores exist larger than 10nm. No correlation between the reaction time or the MF opacity was found with the BET surface area or BJH pore diameter. This can be seen in Figs. 3.9 and 3.10. The surface area of the samples was averaged from three measurements and is between 700 and 1500$m^2/g$, with a few outliers as high as 2000$m^2/g$. Comparing SEM images does not provide any explanation as to the source of these outliers, since the samples have no defining features. The outliers in surface area are likely a result of the carbonization/activation process, in which the pores formed better or worse than normal. The BJH pore diameter of the samples was found to be between 2.5 and 7.2nm.

## 3.3 Raman Spectroscopy

Raman spectra was obtained with a 488nm laser at 10% power using exposure times of 10 and 40 seconds. The resulting spectra is shown in Fig. 3.11, where the G- and D-Raman peaks can be seen at 1580 and 1350$cm^{-1}$ respectively. By comparing each peak, the carbon spheres were estimated to be 8% graphitic.

## 3.4 Conductivity

To determine the conductivity of the carbon material, the sample is placed in series with a DC voltage source and a known resistor. The resistance of the carbon is then given by Eqn. (2.4). By plotting the voltages across the resistor

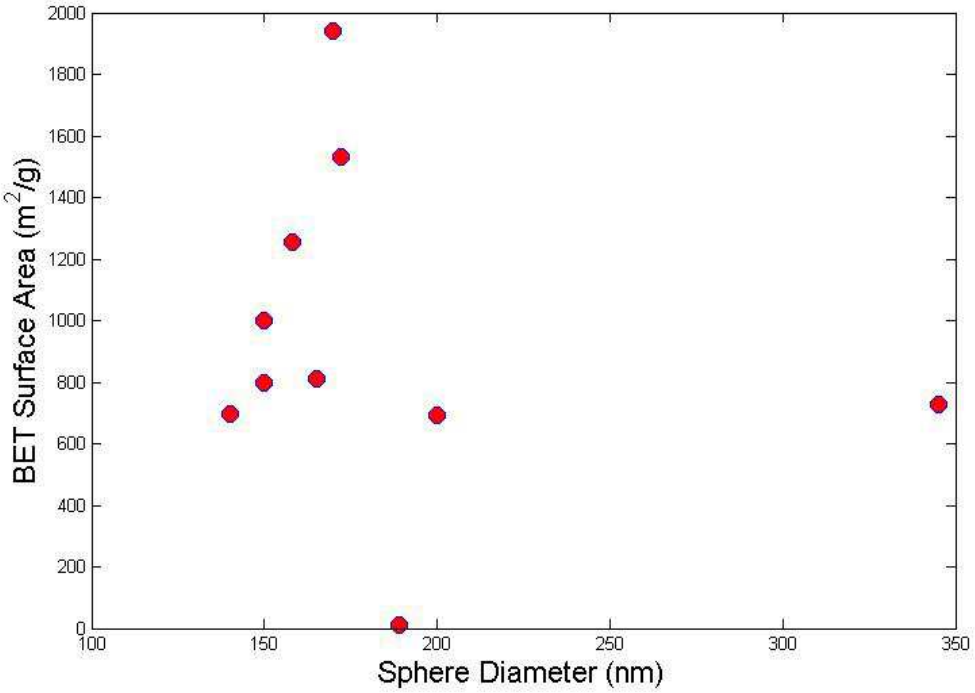


Figure 3.10: The BET surface area was compared to the actual sphere size achieved, and no correlation was found. This is due in part to the lack of variety in the final sphere diameter across samples.

and the sample (Fig. 3.12) and applying least squares fitting, the ratio of the resistances $R$ and $R_{carbon}$ can be found. From this and the dimensions of the sample, the conductance can be calculated.

This procedure was used to analyze samples 3, 6, and 9. Table 3.1 shows the resulting calculated values. The conductivities for the carbon samples were found to be slightly lower than the expected values found in literature for carbon. Graphitic carbon is expected to have a conductivity of $3.0 \times 10^5$S/m, while a value of $2.0 \times 10^3$S/m is expected for amorphous carbon[24]. According the Raman spectral analysis, the carbon is made up of approximately 8% graphitic and 92% amorphous carbon. The conductivity should therefore be somewhere

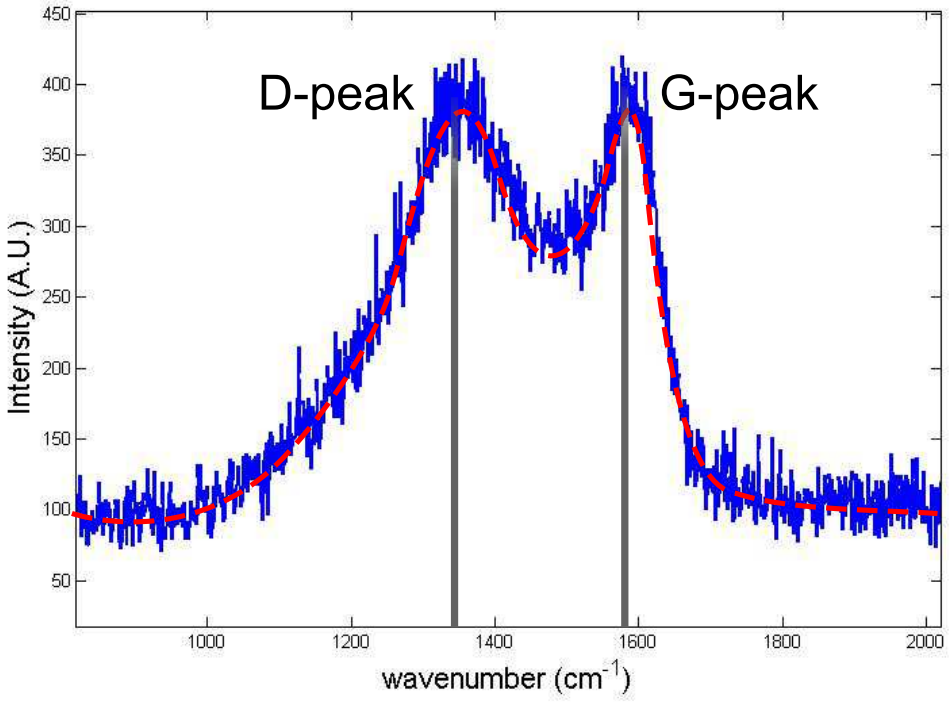


Figure 3.11: Raman spectra obtained for the carbon spheres shows the D- and G-band peaks. The relative intensity of the two peaks indicates that the carbon is approximately 8% graphitic.

between $3.0 \times 10^5$ and $2.0 \times 10^3$S/m. The actual conductivity was measured to be between $0.62 \times 10^3$ and $1.27 \times 10^3$S/m.

## 3.5 Battery Capacity

Battery performance of the porous carbon sphere electrodes was measured by assembling them into coin cells, using the sulfur-infused carbon as the cathode opposite a lithium anode. Three different samples were selected from the synthesized carbon which showed the most promise as a battery material due to their physical and electrical characteristics, namely high surface area, powdery

Table 3.1: The ratio of a known resistance $R$ to the resistance of a carbon sample $R_{carbon}$ is found by comparing the voltage across each resistor. From this, the conductance $\sigma_{carbon}$ of the carbon sample can be found.

| | $R_{carbon}/R$ | $R_{carbon}$ ($\Omega$) | $\sigma_{carbon}(S/m)$ |
|---|---|---|---|
| Sample 3 | $5.1 \times 10^{-3}$ | 77.83 | 620 |
| Sample 6 | $2.5 \times 10^{-3}$ | 38.15 | 1270 |
| Sample 9 | $4.2 \times 10^{-3}$ | 64.09 | 760 |

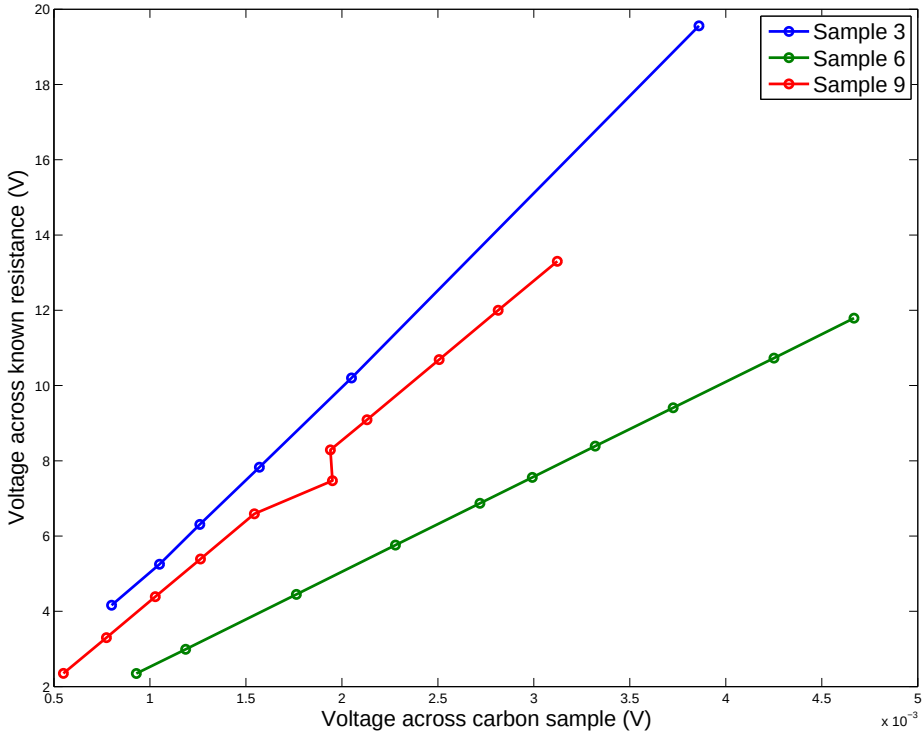


Figure 3.12: The slope of the line produced by plotting the voltages across the resistor and carbon sample gives the ratio of the resistance across the two. Knowing the value of the resistor, the resistance of the carbon sample can be determined and used to calculate the conductance of the material.

consistency, and good electrical conductivity. The materials chosen were from samples 3, 6, and 9 from the final round of synthesis. Electrodes were assembled into batteries using the method previously described, and the coin cells were galvanostatically cycled between 1.7V and 2.8V[27]. Samples 3 and 6 both produced cells with initial voltages ranging from 0.0V to 2.4V. Cells produced from sample 9 showed negligibly low voltage upon assembly. Cells measuring 2.1V or higher were charged and discharged at a rate of 1C over 250 cycles. The resulting capacity values can be seen in Fig.3.13. Sample 3 showed an initial capacity of 843mAh/g, dropping to 271mAh/g after 100 cycles and 125mAh/g after 250. Sample 6 showed better performance at 1160, 305, and 343mAh/g, respectively. The high initial capacity is due to the addition of the irreversible decomposition reaction of the electrolyte[33]. The measured capacity of sample 6 showed a slight upward trend after plateauing, possibly due to the exposure of sulfur infused into the interior of the spheres. Cells from sample 3 continued to be charged and discharged through 1000 cycles to further test its performance. After declining to 25% of the initial capacity by cycle 400, the capacity remained steady, oscillating slightly about 100maH/g, as seen in Fig. 3.14.

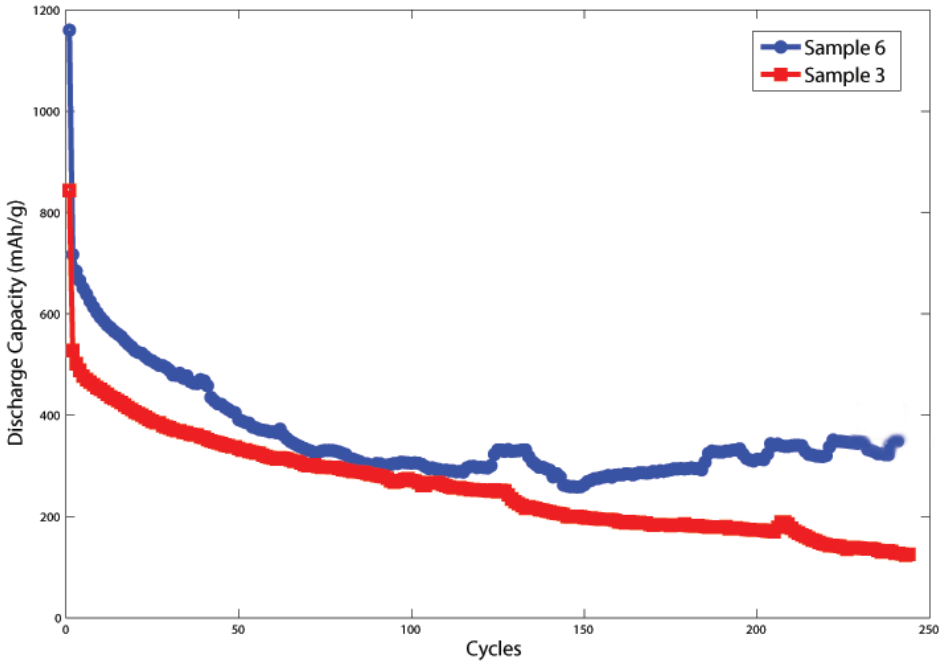


Figure 3.13: Battery performance of porous carbon spheres as sulfur composite electrodes in lithium sulfur batteries shows sharp dropoff of the initial capacity, followed by a slow decline. Charge and discharge cycles were performed at 1C.

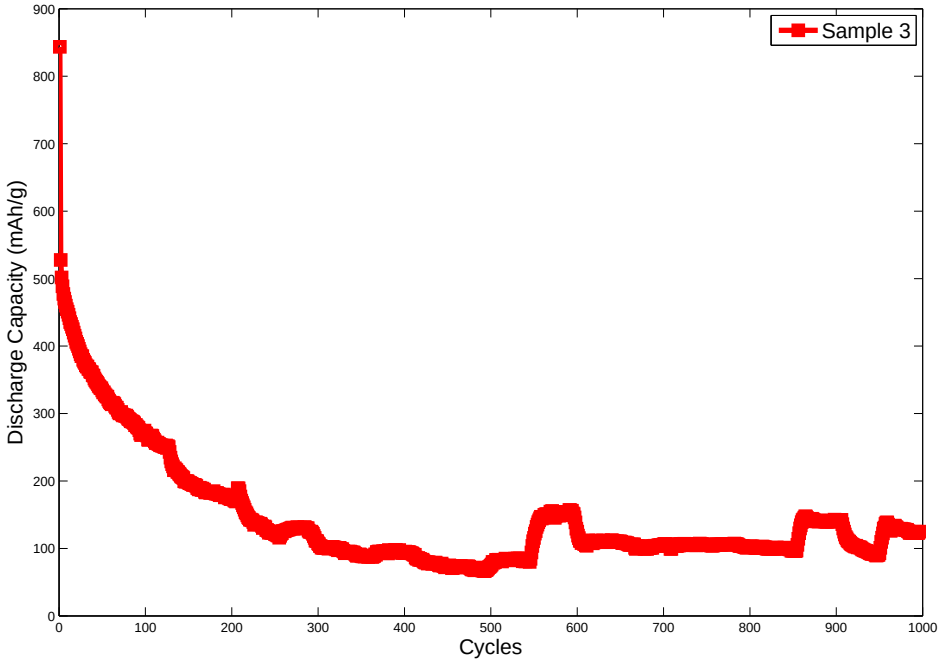


Figure 3.14: Measuring the capacity over 1000 cycles shows decreasing capacity over first 400 cycles, ultimately declining from and initial capacity of 843mAh/g to a steady value of 100mAh/g.

# CHAPTER 4

# CONCLUSION

A synthesis method using self-assembling polymer spheres was developed to synthesize hollow carbon spheres with the intention of using them as the sulfur support in lithium sulfur batteries. The method relies on the self-assembly of resorcinol-formaldehyde spheres, which are encapsulated by melamine-formaldehyde before being freeze dried. After analyzing the carbon, it was found that the spheres were not hollow, but porous throughout. There are several theories which could explain the lack of a hollow core in the spheres. It is possible that the MF prepolymer which forms the inner core is dissolved by the addition of ethanol with the RF solution. This would allow the RF to form independent spheres which become consistently microporous throughout. Another possibility is that the RF simply forms it's own spheres in addition to the MF rather than forming a shell around the prepolymer. This is evidenced by the murky, sometimes opaque liquid found occasionally after filtering the solution. This could be the MF polymer spheres passing through the filter, implying that they are smaller than the 50$\mu$m filter paper pores.

The resulting material still has promising characteristics for use in lithium sulfur cathodes, including surface area as high as 1939$m^2/g$ and pore diameters ranging from 25 to 72nm. SEM imaging showed that most of the spheres produced were between 150 and 200nm in diameter with no correlation to the pH, reaction time, or opacity of the pre-polymer solution. The carbon was tested by Raman spectroscopy and found to be approximately 8% graphitic carbon, which is similar to other synthesis methods[13]. Using TEM imaging and x-ray spectral analysis, it was shown that the melt-infusion process successfully allowed

the sulfur to distribute throughout the carbon sphere.

The electrical conductivity of the samples is between 620 and 1270S/m. This is in agreement with previous measurements made using this apparatus, but is slightly below the expected values. This is likely due to the porous nature of that carbon, which could introduce gaps and convolutions in the material which inhibit the flow of electrons.

The long-term capacity of the battery cells were tested using one hour charge/discharge cycles. The initial capacity was found to be between 840 and 1160mAh/g, reducing by 71% after 100 cycles. After 250 cycles, sample 6 maintained its capacity, even showing a slight increase. Sample 3 continued to decrease in capacity until around 400 cycles had been completed, at which point the capacity was 11% of the initial value. No further decrease was measured between cycles 400 and 1000.

Overall, the capacity of the cells were below expectations. Similar procedures were used to produce electrodes using carbon with hierarchical pore size, and these were demonstrated to have initial capacities as high as 1300mAh/g, degrading to 800mAh/g after 100 cycles[27]. This material performed better than the porous spheres on both initial capacity and cycle lifetime, more than doubling the measured capacity found in the spheres after a similar number cycles. One possible explanation for the poor performance of the spheres is the sublimation of the sulfur out of the spheres. Between the electrodes being cast onto the aluminum backing and the assembly into coin cells, the carbon-sulfur composite sat for several weeks in a fume hood. During this time, it is possible that the sulfur sublimated away, resulting in the low performance of samples 3 and 6, and the complete lack of potential found in sample 9[17][31]. Repeating

the electrode casting, battery assembly, and capacity testing could show improved results if carried out in a more accelerated schedule.

The synthesis method can be further tested and developed to produce the desired hollow spheres, starting by varying the amount and timing of the ethanol addition step. Further characterization could be done using x-ray diffraction for the carbon and SEM imaging for the polymer before carbonization. A complete analysis of the samples by Raman spectroscopy could reveal methods by which to increase conductivity and performance of the carbon. Despite the lack of a hollow core, the synthesis method and resulting carbon spheres show promise as a material for use as the sulfur support in lithium sulfur batteries.

## BIBLIOGRAPHY


[1] Peter G. Bruce, Stefan a. Freunberger, Laurence J. Hardwick, and Jean-Marie Tarascon. LiO2 and LiS batteries with high energy storage. *Nature Materials*, 11(02):172–172, 2011.

[2] Yuliang Cao, Xiaolin Li, Ilhan a Aksay, John Lemmon, Zimin Nie, Zhenguo Yang, and Jun Liu. Sandwich-type functionalized graphene sheet-sulfur nanocomposite for rechargeable lithium batteries. *Physical chemistry chemical physics : PCCP*, 13(17):7660–7665, 2011.

[3] Lithium Sulfur Cells, Liwen Ji, Mumin Rao, Haimei Zheng, Liang Zhang, O Yuanchang Li, and Wenhui Duan. Graphene Oxide as a Sulfur Immobilizer in High Performance Lithium/Surfur cells. *Journal of the American Chemical Society*, 133:18522–18525, 2011.

[4] Sang-Eun E Cheon, S K Ko, Ji-Hoon H Cho, Sun-Wook W Kim, Eog-Yong Y Chin, Hee-Tak T Kim, Ki-Seok Ko, Ji-Hoon H Cho, Sun-Wook W Kim, Eog-Yong Y Chin, Hee-Tak T Kim, S K Ko, Ji-Hoon H Cho, Sun-Wook W Kim, Eog-Yong Y Chin, and Hee-Tak T Kim. Rechargeable Lithium Sulfur Battery. *Journal of The Electrochemical Society*, 150(6):A800–A805, 2003.

[5] Donald A. Dornbusch, Ramsey Hilton, Michael J. Gordon, and Galen J. Suppes. Effects of carbon surface area on performance of lithium sulfur battery cathodes. *Journal of Industrial and Engineering Chemistry*, 19(6):1968–1972, 2013.

[6] Scott Evers, Taeeun Yim, and Linda F Nazar. Understanding the Nature of Absorption/Adsorption in Nanoporous Polysul fi de Sorbents for the Li S Battery. *Journal of Physical Chemistry C*, (116):19653–19658, 2012.

[7] Juchen Guo, Yunhua Xu, and Chunsheng Wang. Sulfur-Impregnated Disordered Carbon Nanotubes Cathode for Lithium Sulfur Batteries. *NanoLetters*, pages 4288–4294, 2011.

[8] Yu Han and Jackie Y. Ying. Generalized fluorocarbon-surfactant-mediated synthesis of nanoparticles with various mesoporous structures. *Angewandte Chemie - International Edition*, 44(2):288–292, 2004.

[9] N. Jayaprakash, J. Shen, Surya S. Moganty, A. Corona, and Lynden A. Archer. Porous hollow carbon@sulfur composites for high-power lithium-sulfur batteries. *Angewandte Chemie - International Edition*, 50(26):5904–5908, 2011.

[10] Xiulei Ji, Scott Evers, Robert Black, and Linda F Nazar. Stabilizing lithium-sulphur cathodes using polysulphide reservoirs. *Nature communications*, 2(May):325, 2011.

[11] Jin Jin, Norikazu Nishiyama, Yasuyuki Egashira, and Korekazu Ueyama. Pore structure and pore size controls of ordered mesoporous carbons prepared from resorcinol/formaldehyde/triblock polymers. *Microporous and Mesoporous Materials*, 118(1-3):218–223, 2009.

[12] Kisuk Kang. Electrodes with High Power. *Science*, 311(5763):977–980, 2006.

[13] Chy Hyung Kim, Dong Keun Lee, and Thomas J. Pinnavaia. Graphitic mesostructured carbon prepared from aromatic precursors. *Langmuir*, 20(13):5157–5159, 2004.

[14] Tae-wan Kim, In-soo Park, and Ryong Ryoo. A Synthetic Route to Ordered Mesoporous Carbon Materials with Graphitic Pore Walls.pdf. *Angewandte Chemie - International Edition*, (115):4511–4515, 2003.

[15] Barnaby D.A. Levin, Michael J. Zachman, Jörg G. Werner, Ulrich Wiesner, Lena F. Kourkoutis, and David A. Muller. Characterizing Sulfur in TEM and STEM, with Applications to Lithium Sulfur Batteries. *Microscopy and Microanalysis*, 20(S3):446–447, 2014.

[16] Xiaolin Li, Yuliang Cao, Wen Qi, Laxmikant V. Saraf, Jie Xiao, Zimin Nie, Jaroniec Mietek, Ji-Guang Zhang, Birgit Schwenzer, and Jun Liu. Optimization of mesoporous carbon structures for lithiumsulfur battery applications. *Journal of Materials Chemistry*, 21(41):16603, 2011.

[17] Zhen Li, Lixia Yuan, Ziqi Yi, Yongming Sun, Yang Liu, Yan Jiang, Yue Shen, Ying Xin, Zhaoliang Zhang, and Yunhui Huang. Insight into the electrode mechanism in lithium-sulfur batteries with ordered microporous carbon confined sulfur as the cathode. *Advanced Energy Materials*, 4(7):1–8, 2014.

[18] Xiao Liang, Zhaoyin Wen, Yu Liu, Hao Zhang, Lezhi Huang, and Jun Jin. Highly dispersed sulfur in ordered mesoporous carbon sphere as a composite cathode for rechargeable polymer Li/S battery. *Journal of Power Sources*, 196(7):3655–3658, 2011.

[19] Jian Liu, Shiyang Bai, Hua Zhong, Can Li, and Qihua Yang. Tunable assembly of organosilica hollow nanospheres. *Journal of Physical Chemistry C*, 114(2):953–961, 2010.

[20] Jian Liu, Sandy Budi Hartono, Yong Gang Jin, Zhen Li, Gao Qing (Max) Lu, and Shi Zhang Qiao. A facile vesicle template route to multi-shelled mesoporous silica hollow nanospheres. *Journal of Materials Chemistry*, 20(22):4595–4601, 2010.

[21] Jian Liu, Tianyu Yang, Da-Wei Wang, Gao Qing (Max) Lu, Dongyuan Zhao, and Shi Zhang Qiao. A facile soft-template synthesis of mesoporous polymeric and carbonaceous nanospheres. *Nature Communications*, 4:2798, 2013.

[22] Riley Mikhaylik, Yuriy and Kovalev, Igor and Xu, Jason and Schock. Rechargeable Li-S Battery with Specific Energy 350Wh/kg and Specific Power 3000W/kg. *ECS Transactions*, 13(19):53–59, 2008.

[23] Panasonic. NCR18650.

[24] Hugh O Pierson. Handbook of carbon, graphite, diamonds and fullerenes: Processing, properties and applications (materials science and process technology). *William Andrew Inc*, 1993.

[25] MLB Rao. Organic electrolyte cells. *US Patent 3,413,154*, 1968.

[26] By Ryong Ryoo, Sang Hoon Joo, Michal Kruk, and Mietek Jaroniec. Ordered Mesoporous Carbons **. *Advanced Materials*, 13(9):677–681, 2001.

[27] Ritu Sahore, Luis P. Estevez, Anirudh Ramanujapuram, Francis J. Disalvo, and Emmanuel P. Giannelis. High-rate lithium-sulfur batteries enabled by hierarchical porous carbons synthesized via ice templation. *Journal of Power Sources*, 297:188–194, 2015.

[28] Ritu Sahore, Barnaby D A Levin, Mian Pan, David A Muller, Francis J Disalvo, and Emmanuel P Giannelis. Design Principles for Optimum Performance of Porous Carbons in Lithium Sulfur Batteries. *Advanced Energy Materials*, 201600134:1–9, 2016.

[29] Min-Sang Song, Sang-Cheol Han, Hyun-Seok Kim, Jin-Ho Kim, Ki-Tae Kim, Yong-Mook Kang, Hyo-Jun Ahn, S X Dou, and Jai-Young Lee. Effects of Nanosized Adsorbing Material on Electrochemical Properties of Sulfur Cathodes for Li/S Secondary Batteries. *Journal of The Electrochemical Society*, 151(6):A791—-A795, 2004.

[30] Shunsuke Tanaka, Norikazu Nishiyama, and Yasuyuki Egashira. Synthesis of ordered mesoporous carbons with channel structure from an organic-

organic nanocomposite. *Chemical communications (Cambridge, England)*, (16):2125–2127, 2005.

[31] Soeren Thieme, Jan Brueckner, Andreas Meier, Ingolf Bauer, Katharina Gruber, Joerg Kaspar, Alexandra Helmer, Holger Althues, Martin Schmuck, and Stefan Kaskel. A lithium-sulfur full cell with ultralong cycle life: influence of cathode structure and polysulfide additive. *Journal of Materials Chemistry A*, 3(7):3808–3820, 2015.

[32] Da-Wei Wang, Guangmin Zhou, Feng Li, Kuang-Hsu Wu, Gao Qing, Max Lu, Hui-Ming Cheng, and Ian R Gentle. A microporousmesoporous carbon with graphitic structure for a high-rate stable sulfur cathode in carbonate solvent-based LiS batteries. *Phys. Chem. Chem. Phys. Phys. Chem. Chem. Phys*, 14(14):8703–8710, 2012.

[33] Zhi Wei Seh, Weiyang Li, Judy J Cha, Guangyuan Zheng, Yuan Yang, Matthew T McDowell, Po-Chun Hsu, and Yi Cui. Sulphur-TiO2 yolk-shell nanoarchitecture with internal void space for long-cycle lithium-sulphur batteries. *Nature communications*, 4:1331, 2013.

[34] Lifen Xiao, Yuliang Cao, Jie Xiao, Birgit Schwenzer, Mark H. Engelhard, Laxmikant V. Saraf, Zimin Nie, Gregory J. Exarhos, and Jun Liu. A soft approach to encapsulate sulfur: Polyaniline nanotubes for lithium-sulfur batteries with long cycle life. *Advanced Materials*, 24(9):1176–1181, 2012.

[35] H. Yamin and E. Peled. Electrochemistry of a nonaqueous lithium/sulfur cell. *Journal of Power Sources*, 9(3):281–287, 1983.

[36] Huan Ye, Ya-Xia Yin, Sen Xin, and Yu-Guo Guo. Tuning the porous structure of carbon hosts for loading sulfur toward long lifespan cathode materials for LiS batteries. *Journal of Materials Chemistry A*, 1(22):6602–6608, 2013.

[37] B. Zhang, C. Lai, Z. Zhou, and X. P. Gao. Preparation and electrochemical properties of sulfur-acetylene black composites as cathode materials. *Electrochimica Acta*, 54(14):3708–3713, 2009.

[38] Shi Chao Zhang, Lan Zhang, Wei Kun Wang, and Wen Juan Xue. A Novel cathode material based on polyaniline used for lithium/sulfur secondary battery. *Synthetic Metals*, 160(17-18):2041–2044, 2010.

[39] J. Zheng, M. Gu, M. J. Wagner, K. A. Hays, X. Li, P. Zuo, C. Wang, J.-G.

Zhang, J. Liu, and J. Xiao. Revisit Carbon/Sulfur Composite for Li-S Batteries. *Journal of the Electrochemical Society*, 160(10):A1624–A1628, 2013.

[40] W. Zheng, Y. W. Liu, X. G. Hu, and C. F. Zhang. Novel nanosized adsorbing sulfur composite cathode materials for the advanced secondary lithium batteries. *Electrochimica Acta*, 51(7):1330–1335, 2006.